Published in the Proceedings of the 16th International Aluminum Alloys Conference (ICAA16) 2018
ISBN: 978-1-926872-41-4
by the Canadian Institute of Mining, Metallurgy & Petroleum

THE NATURE OF SOLUTE CLUSTERS AND GP-ZONES IN THE Al-Mg-Si SYSTEM

* C. D. Marioara[1], S. J. Andersen[1], J. Friis[1], O. Engler[2] and Y. Aruga[3]

[1]SINTEF Industry
Trondheim, Norway
*(*Corresponding author: calin.d.marioara@sintef.no)*

[2]Hydro Aluminium Rolled Products GmbH, Research and Development Bonn, Germany

[3]Materials Research Laboratory, Kobe Steel
Kobe, Hyogo, Japan

ABSTRACT

This work investigates the early stages of precipitation in Al-Mg-Si alloys using a combination of high angle annular dark field scanning transmission electron microscopy (HAADF-STEM), selected area electron diffraction (SAED) and density functional theory (DFT) calculations. Quenching from a high temperature (solution) treatment leaves an alloy in a high-energy unstable state, with solute and vacancies in supersaturation. Thus, already at room temperature (RT) a large driving force exists for solute atoms to cluster and order on the Al matrix positions. DFT calculations indicate that strain alleviation is important at this stage. We observe larger regions of Mg-dominated $L1_0$ ordering together with a Si-dominated ordering of smaller clusters in a particular geometry connected to the Si-network found in all the precipitates. In addition, building blocks of the main hardening phase β", stabilized by vacancies, are observed at higher, typical pre-aging temperatures.

KEYWORDS

Atomic clusters, Density functional theory, Precipitation, Transmission electron microscopy

INTRODUCTION

Al-Mg-Si (6xxx) alloys are widely used in industry due to a combination of favorable properties such as strength, ductility, corrosion resistance and lightweight. They undergo a complex production route, usually consisting of the following thermo-mechanical steps: casting, homogenization, extrusion or rolling, solution heat treatment (SHT) and artificial aging (AA). The SHT takes place at temperatures above the solvus line in the phase diagram, usually between 500°C and 570°C, followed by a rapid cooling to RT. This ensures that high amounts of solute atoms, uniformly distributed on the cubic face-centered (FCC) Al lattice, together with a large amount of vacancies, are quenched-in. The material is therefore in a super-saturated and unstable state. During the subsequent AA, at temperatures usually between 150°C and 220°C, the solute atoms diffuse and cluster, forming metastable precipitates with needle/ lath/ rod morphologies having the main growth direction along <100>Al. With a maximum alloy solute level (Mg + Si) of only 2%, these precipitates increase material strength up to three times that of pure Al, and are essential for the final material properties. To understand and make better use of this phenomenon, it is imperative to research the nature of the precipitates (such as their atomic structure), measure their key parameters (number density, size, volume fraction) and connect it to material properties (Marioara, Andersen, Zandbergen & Holmestad, 2005; Marioara et al., 2014). The following precipitation sequence is given for the Al-Mg-Si system:

SSSS → Atomic clusters → GP zones → β" (Andersen, Zandbergen, Jansen, Træholt, Tundal & Reiso, 1998; Hasting et al., 2009) → Post-β" (β' (Vissers, van Huis, Jansen, Zandbergen, Marioara & Andersen, 2007), U1 (Andersen, Marioara, Vissers, Frøseth & Zandbergen, 2007), U2 (Andersen, Marioara, Frøseth, Vissers & Zandbergen, 2005), B' (Vissers, Marioara, Andersen & Holmestad, 2008)) → β, Si (stable)

SSSS stands for super-saturated solid solution. β" is the main hardening phase. Post-β" phases form upon over-aging.

An interesting aspect about these alloys is that a RT storage after SHT leads to atomic clustering and significant hardness increase (Pashley, Rhodes & Sendorek, 1966; Yamada, Sato & Kamio, 2000; Røyset, Stene, Sæter & Reiso, 2006; Engler, Schäfer & Myhr, 2014). This Natural Aging (NA) affects precipitate parameters and therefore the mechanical properties after a subsequent AA. In practice, the NA is difficult to avoid. For denser alloys (solute level higher than 1) it has a negative effect, decreasing hardness after the AA, as compared with conditions immediately aged after SHT (Yamada et al., 2000; Wenner, Marioara, Andersen & Holmestad, 2012; Engler et al., 2017). However, a Pre-Aging (PA) at temperatures above 70°C, introduced between SHT and AA, has been shown to suppress this effect (Murali, Arunkumar, Chetty, Raman & Murthy, 1997; Abid, Boubertakh & Hamamda, 2010; Aruga, Kozuka & Sato, 2018). The atomic clusters formed during NA have also been called 'Cluster (1)', and the ones formed during the PA 'Cluster (2)' (Serizawa, Hirosawa & Sato, 2008).

Although attempts have been made to understand their crystallographic nature (Kovarik, Gouma, Kisielowski, Court & Mills, 2004; Matsuda et al., 2017), the small size and high coherency with the Al matrix means clusters escape direct observation by traditional methods such as bright-field TEM and high-resolution TEM. Atom Probe Tomography (APT) studies concluded that composition of clusters formed during NA varies, and most of them do not grow during subsequent AA, while some clusters formed during PA have an Mg/Si ratio near unity and will develop into needle-shaped precipitates during AA (Serizawa, et al., 2008; Aruga, Kozuka, Takaki & Sato, 2014, 2015; Engler et al., 2017). However, due to poor spatial resolution, APT does not provide crystallographic information. Recent developments in TEM imaging techniques such as spherical aberration (Cs) probe corrected HAADF-STEM have brought hopes that direct detection of the atomic clusters is possible. Images formed with this technique are the result of an incoherent electron scattering process and are therefore more directly interpretable. They are generally unaffected by small changes in the objective lens defocus and specimen thickness, have Z-contrast and sub-Ångstrom spatial resolutions (Nellist & Pennycook, 2000; Yamazaki, Kawasaki, Watanabe, Hashimoto & Shiojiri, 2002; Rose, 2010). For these reasons, in the present work the HAADF-STEM technique was

chosen for direct imaging of the cluster-containing conditions. This was combined with SAED to investigate if diffuse electron scattering from such clusters can be detected in diffraction mode.

EXPERIMENTAL

Material for the present study was taken from ~1 mm thick sheets of the Al-Mg-Si alloy AA 6016 with composition (wt%) 1.23 Si, 0.30 Mg, 0.04 Cu, 0.19 Fe and 0.06 Mn. The sheets were produced by conventional hot and cold rolling. Lab-sized samples were SHT for 5 min at 560°C and subsequently water quenched. One set of samples, referred to as material 'NA' hereafter, was naturally aged between one to three months. The other set of samples, 'PA', was pre-aged for 24 h at 90°C immediately after the SHT.

TEM specimens were electropolished with a TenuPol-5 machine, using a mixture of 1/3 HNO_3 and 2/3 methanol kept at -25°C, and a voltage of 20 V. A double aberration-corrected (image and probe Cs) cold-FEG Jeol ARM-200F operated at 200 kV was used for the HAADF-STEM imaging. The probe size was 0.08 nm, the convergence semi-angle was 28 mrad and the inner and outer collection angles were 35 and 150 mrad, respectively. The inner collection angle is somewhat smaller than what is considered for HAADF-STEM (50 mrad), but our experience is that the lower Z-contrast Mg-containing atomic columns are better resolved with this setting. Large scans have been recorded, with 2048 by 2048 pixels, 19.35 μs pixel time and 65.2 pixels per nm resolution. SAED patters were recorded with a Jeol JEM-2100 TEM equipped with a LaB_6 filament and operated at 200 kV. An Orius SC 200D CCD camera was used for the recordings. A SAED pattern consists of a summation of 20 individual exposures of 15 s each. A 10 μm diameter condenser aperture and the largest selected area aperture (120 μm) were used, with maximum beam spread. This overexposes Al spots, but clarifies the weak diffuse scattering from atomic clusters. For the DFT calculations, formation enthalpies of different solute configurations were calculated using the Vienna *ab initio* simulation package (VASP) (Kresse & Furthmuller, 1996; Kresse & Hafner, 1993), applying the projector augmented wave method within the Perdew-Burke-Ernzerhof (PBE) generalized gradient approximation (Perdew, 1996). The plane wave energy cut-off was 400 eV and a Γ-centered 3×3×9 k-points mesh were used, corresponding to a maximal k-point distances of 0.18 $Å^{-1}$ in each direction. The electronic accuracy for self-consistent loops was set at 10^{-6} eV. The atomic positions were relaxed to a maximum force of 0.001 eV/Å between atoms, using first-order Methfessel-Paxton for smearing of partial occupation and a smearing factor of 0.2. For accurate energies, we conducted a separate calculation using the tetrahedron method with Blöchl correction for the smearing. The DFT calculations were performed in periodic slabs consisting of 4×4×1 Al FCC unit cells (64 atoms) with lattice parameter relaxed to a = 4.0400 Å. Hence, we assume full periodicity along the [001]Al "viewing" direction. The formation enthalpies were calculated as

$$\Delta H = E_{Al_l Mg_m Si_n} - \left(lE_{Al} + mE_{Mg} + E_{Si}\right), \quad where\ l + m + n = 64.$$

$E_{Al_l Mg_m Si_n}$ is the energy of a slab with l, m and n Al, Mg and Si atoms, respectively. $E_{Al} = E_{Al_{64}}/64$ is the energy of an Al atom in solid solution. E_{Mg} and E_{Si} correspond to the energy per atom for a row Mg and Si atoms respectively, along the [001]Al direction. Hence $E_X = E_{Al_{63}X} - 63E_{Al}$, with $X = Mg, Si$.

RESULTS

A crucial observation, and catalyst for the present work, was the detection of diffuse scattering spots in SAED patterns of the NA conditions, which corresponded with spots present in Fast Fourier Transforms (FFT) of HAADF-STEM images. Figure 1 illustrates this with examples recorded in an <100>Al zone axis (a to c) and <110>Al zone axis (d to f). It indicates that atomic clusters responsible for the diffuse scattering in SAED patterns generate weak Z-contrast modulations in the HAADF-STEM images. Therefore, by choosing selected spots in the FFT pattern, and performing an inverse FFT (IFFT), structural information about the clusters could be obtained. In <100>Al projection we identified two sets of spots in the FFT and SAED patterns, corresponding to numbers '1' (in the forbidden 110Al positions) and '2' (four weaker spots surrounding 110Al spots in a square arrangement, nearer the extinct 100Al

positions), shown in one quadrant in the indexed SAED pattern in Figure 1c. Two sets of spots, marked as '3' and '4' in Figure 1f, are also identified in patterns of the <110>Al projection. The set '3' appears as satellite spots to 220Al. IFFT images obtained by selecting the different sets of spots with a mask tool are shown in Figure 2. Figure 2a and b show IFFT images obtained by choosing the '1' and the '2' sets of spots, respectively.

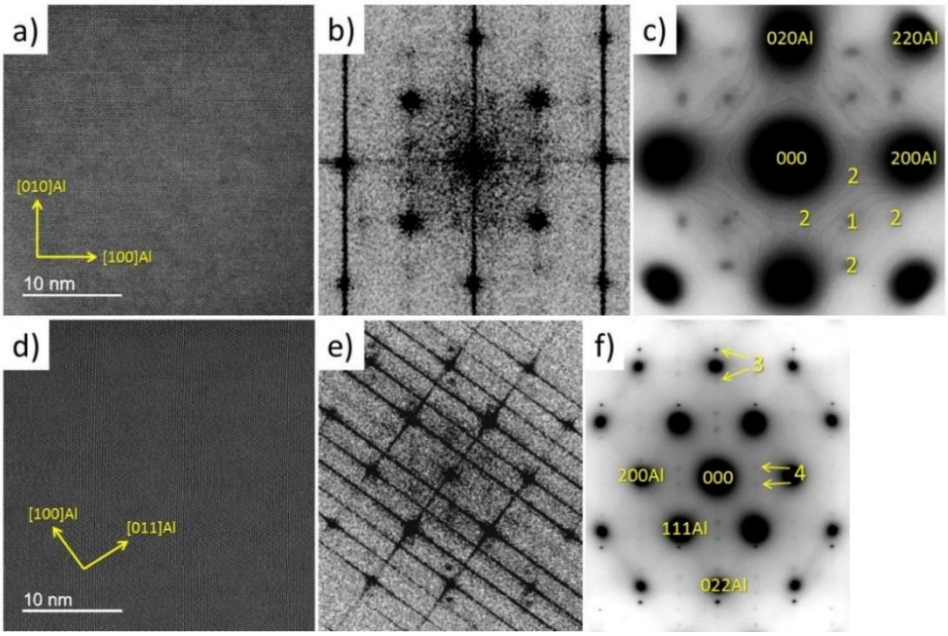

Figure 1. NA condition. a) Raw HAADF-STEM image, b) corresponding FFT pattern and c) SAED pattern, all in <100>Al. FFT and SAED patterns show same spots (1, 2). d) Raw HAADF-STEM image in <110> Al. e) Corresponding FFT pattern and f) SAED pattern. Same spots are present in both FFT and SAED (3,4), as indexed in (f). Stripes between Al spots in b), e) are caused by scanning noise.

Selection of spot '1' yields an IFFT image with large domains that could extend more than 10 nm, with a contrast consistent with an $L1_0$ type of ordering on the FCC Al lattice. Antiphase boundaries (APBs) separate the domains, as indicated by yellow lines in Figure 2a. The IFFT image created by selecting the second set ('2') in the FFT is different, and shows much finer clusters (2 to 4 nm in diameter). Careful visual analysis of several clusters shows that the high contrast atomic columns connect as triangles and squares, in a fashion resembling a σ- type Frank-Kasper (FK) phase (Frank & Kasper, 1958). We notice that a single fundamental unit suffices to explain the build-up of this phase. It is a square-based pyramid on the FCC Al lattice, spanning one Al cell: The base atoms are corners of one face of the Al unit cell, the top being the face center of the opposite side of the cube. In an <100>Al projection we can occasionally discern the base edge-on, with high Z-contrast atoms occupying the corners of the base of an Al unit cell, and some lower intensity for the top. Normally, along the viewing direction the regions overlap with clusters of the other rotations or translations. However, the model seems to explain all overlap situations. The IFFT image in Figure 2c is obtained by using spots '3' as well as the adjacent 022Al spots. It shows domains with sizes that can exceed 5 nm. Within each domain a modulation of the lattice spacing appears, as waves along the <011>Al direction, each wave with 3 to 4 d_{220}^{Al} width (0.4 to 0.6 nm) and a wavelength (periodicity) of $7d_{220}^{Al}$ ~ 1 nm. The IFFT image in Figure 2d is formed by set '4' spots and shows a different pattern, which consists of more localized clusters of diameter 2 to 4 nm, which match collections of base-to-base FK pyramids described above, when viewed along <011>Al.

Based on these observations, we conclude there are two types of ordering on the Al FCC lattice. The first ordering corresponds to spot sets '1' and '3' in the SAED and FFT patterns, and originates from

larger domains of $L1_0$ ordering, separated by APBs. This ordering appears to be modulated as density waves along <110>Al directions. A similar observation was reported in binary Al - 10 wt% Mg alloys during NA (Sato, Kojima & Takahashi, 1982). In that case, ordering was of $L1_2$ type with density waves along <100>Al directions, and one order of magnitude larger wave width and wavelength. The similarity supports our conclusion that Mg is behind the $L1_0$ ordering observed in the present work. As the Mg solute concentration in a typical 6xxx alloy is below 1%, there is insufficient Mg to fill in all $L1_0$ atomic positions. Instead, we suggest the existence of a diluted, average $L1_0$ type ordering in these alloys, with concentration fluctuating as density waves. Both Sato's et al. (1982) and our work indicate that such Mg-induced modulated structures are formed by spinodal decomposition.

Regarding the ordering that generates spots '2' and '4', it is interesting to notice that the square-based pyramid described above is an integral part of all precipitate-types found in the 6xxx system, including the equilibrium β phase and diamond Si, and is defined by 5 Si atoms. It is the building block of the so-called 'Si-network' in all metastable precipitates, where Si columns project as a near-hexagonal symmetry viewed along the needle direction (Andersen et al., 2004, 2007). Therefore, we conclude the atomic clusters shown in Figure 2b, d, assumed to be a collection of pyramids and ordered as a FK structure, are in fact the same type of Si pyramids on the Al lattice that build the Si-network in all the precipitate phases in the Al-Mg-Si system.

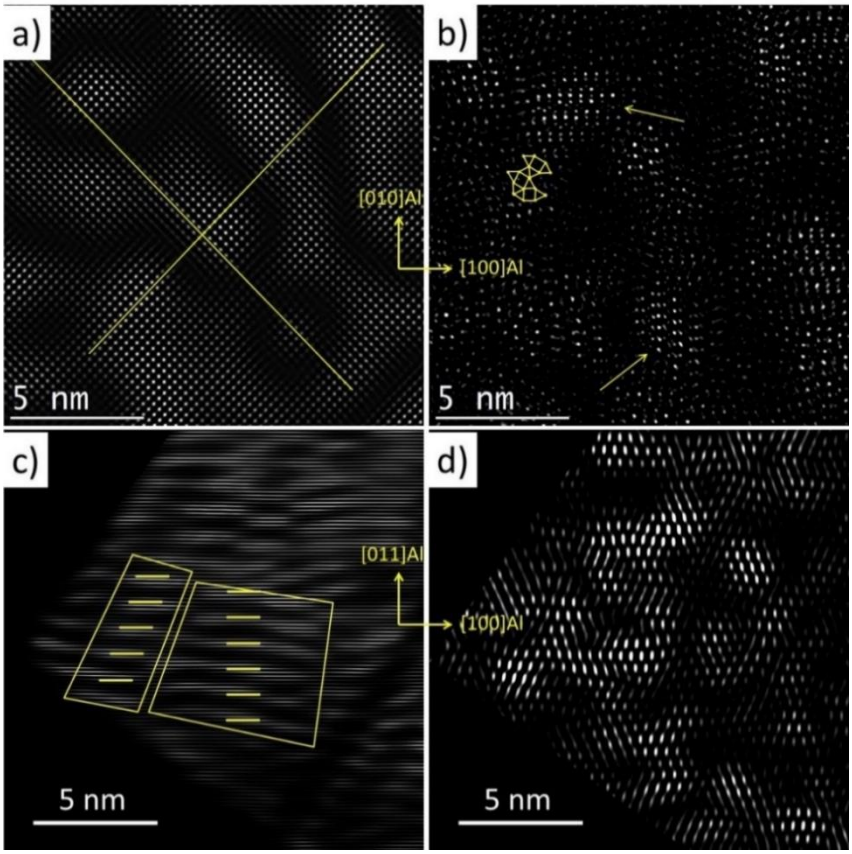

Figure 2. IFFT images based on spots 1 (a)), 2 (b)), 3 (c)) and 4 (d)), referring to indexing in Figure 1c, f. a): Domains interpreted as $L1_0$ modulation on the FCC Al lattice. Anti-phase boundaries separate the domains (seen by a phase-shift when following a line across a boundary). b): Overlay showing small clusters with high contrast atomic columns in groups of triangles and squares, in a σ-type Frank-Kasper (FK) fashion. Arrows: overlapped FK clusters. c) Two domains indicate same wave modulation along <110>Al (with ~ 1 nm ~ $7d_{220}^{Al}$ periodicity). d) shows more localized clusters with sizes similar as in b).

Similar analysis as above was performed in the PA condition. In Figure 3a the diffuse spots in the SAED from this condition show that both orderings found in the NA conditions are still present. However, additional streaks develop between the 000 and 200 type Al spots indicating that needle-shaped precipitates form with growth direction along <100>Al. HAADF-STEM images show these precipitates to be molecules of the β" phase, each molecule comprising a structure called 'the eye'. Both single eyes and small groups of eyes can exist (Figure 3b-d). The figure shows the eyes arrange along <310>Al and <320>Al, forming fractional β" unit cells, see Figure 3c, d. Four (unshared) eyes would span half β" unit cell (when shared, only two define a cell). The figure can illustrate how β" phase builds up.

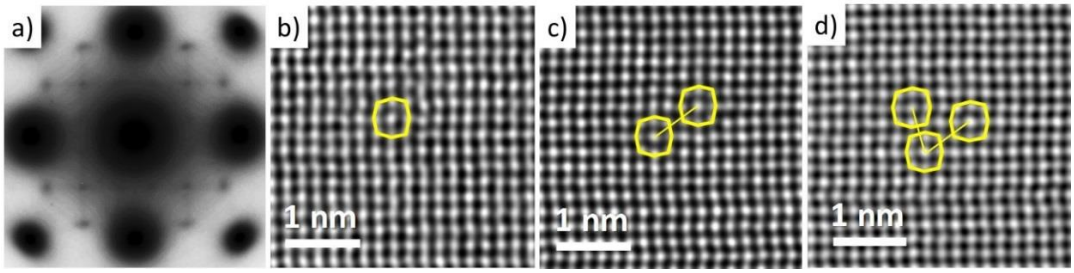

Figure 3. a) SAED pattern from the PA condition. b) - d) HAADF-STEM images from the PA condition showing cross-sections of fractional β" unit cells in the <001>Al projection.

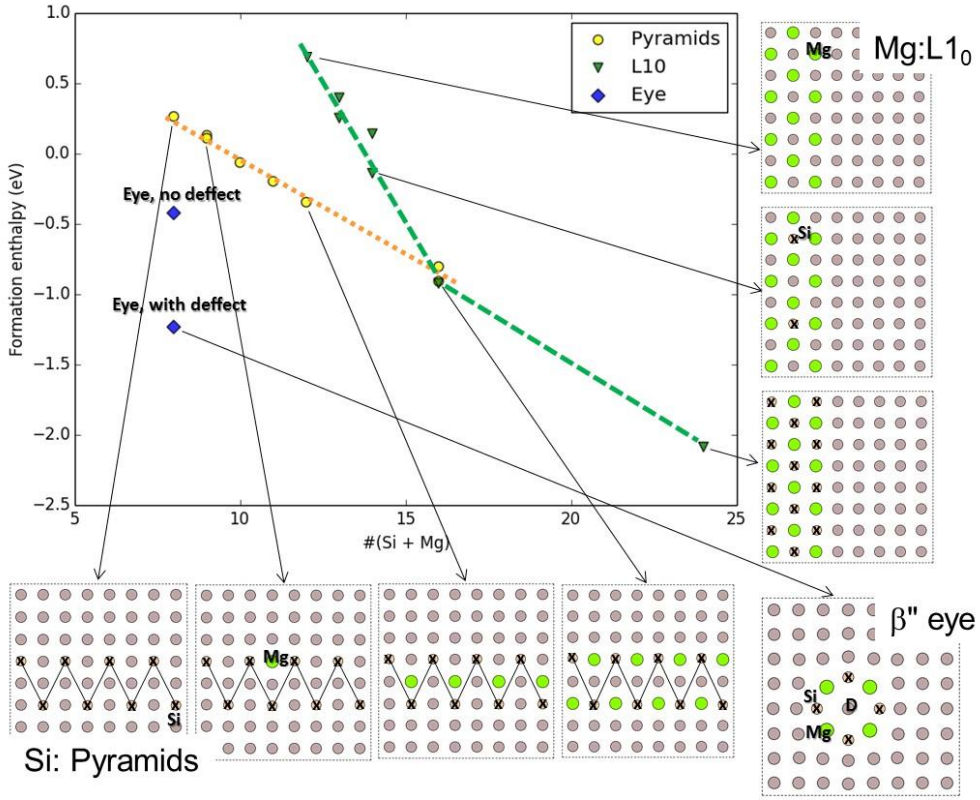

Figure 4. DFT calculation of formation enthalpies for different $L1_0$ and pyramid orderings, as well as for one β" eye, with and without the defect. Energy is reduced by addition of Si to the $L1_0$ ordered Mg (see the dashed line), by addition of Mg to the Si pyramid ordering (see the dotted line), and by creating a 1D defect in the center of an eye.

SAED was also performed in two binary alloys; Al - 1.3 at% Si and Al - 1 wt% Mg, in both as-extruded + NA and SHT + NA conditions. Here the diffuse spots were absent, indicating that, although the Mg and Si orderings in Al-Mg-Si alloys look very distinct, stabilization requires both elements. This assumption was tested by DFT calculations, where Si atoms were gradually added to a Mg $L1_0$ ordering, and Mg was gradually added to a row of Si pyramids. In addition, the stability of one β" eye was tested, as seen in Figure 4. The β" phase can be considered as a superstructure in Al. The main structural difference concerns the center columns of the eyes (Mg1 site), with (Al or Mg) atoms that are interstitial – thus an eye is a one-dimensional (1D) defect. Each defect requires a vacancy to form to avoid too near atoms in the front (Andersen, Marioara, Friis, Bjørge, Du & Ringdalen, 2017). Therefore, the formation enthalpy of a single eye with and without the defect was considered. The following observations can be drawn from Figure 4:

- Adding Si to the Mg $L1_0$ ordering, and adding Mg to the pyramid ordering reduces the energy of the respective ordering. This supports the experimental observations that such orderings do not exist in binary alloys with similar Mg or Si concentrations. As Mg is a larger atom and Si a smaller atom than Al, strain alleviation must be an important factor for the observed energy reduction.
- The 1D defect greatly reduces energy of the constituent β" molecules. Such molecules were only observed in the PA conditions. As the alloy evolution during AA is towards formation of β" needles, we conclude that the fractional β" units observed in the PA conditions are nuclei of the β" phase.

CONCLUSIONS

This work finds that upon NA the solute atoms order on the Al FCC lattice in two main configurations. One type is driven by Mg and consists of large domains of average $L1_0$ atomic arrangement. The domains may extend several nm and are separated by antiphase boundaries, where domains based on the two different sets of {100}Al planes meet. Within each domain there are density waves along <110>Al, with approximately 1 nm wavelength. The other ordering is governed by Si, which arranges in pyramids having as base the corners of a face in the Al unit cell, and the top atom is in the middle of the opposite face. These pyramids arrange in an FK σ-type manner, giving rise to Si-rich clusters with 2 to 4 nm size. Although experimental data and DFT calculation indicate that both Mg and Si atoms are needed to stabilize each-other's ordering, so far no coupling or co-clustering was detected between the two orderings. Both orderings lock the Mg and Si atoms into stable configurations that cannot grow, and will delay the formation of β" during a subsequent AA. Therefore, the orderings can explain the reported negative effect of NA. However, since only the Si ordering gives more localized atomic clusters, we considered them to be the 'real' clusters that form during NA.

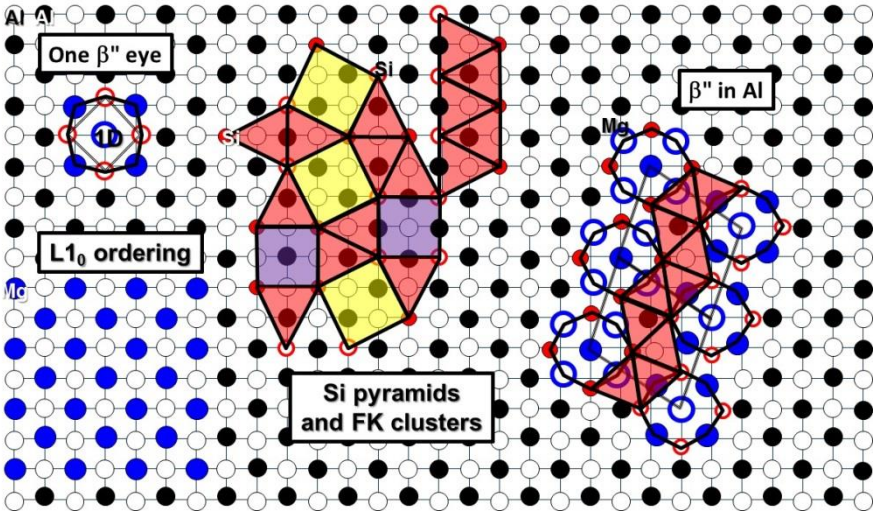

Figure 5. Al FCC lattice as viewed along [001]Al, presenting Mg $L1_0$ ordering, Si FK σ-ordering, a β" eye and a half β" cell repeated along <130>Al. According to their reported effect on delaying nucleation and growth of β" needles during AA, the $L1_0$ and FK orderings can be associated with clusters with variable Mg/Si ratio. On the contrary, β" eyes develop into β" phase during AA, and can be linked to clusters with Mg/Si ~ 1. A 1D defect (indicated in the middle of the β" eye) is needed to break the symmetry of the Al FCC lattice and form one eye.

The above orderings are also found in the PA conditions. However, due to the higher temperatures upon PA, 1D defects form in the matrix, which allow formation of β" constituent molecules (eyes). As PA conditions rapidly develop into β" type microstructures during subsequent AA, we conclude that β" eyes represent the clusters with a Mg/Si ratio near one. Figure 5 is a schematic drawing with NA orderings, a single β" eye and a repeated semi-cell of β" along a <130>Al direction, on the FCC Al matrix viewed along [001]Al.

ACKNOWLEDGMENTS

We thank Hydro Al and the Research Council of Norway for support through the BIA 'RolEx' project (Grant 219371), the Hydro Fond project 'Understanding and multi-scale modelling of early stage precipitation in age hardenable Al-Mg-Si alloys' at Sintef, and Hydro Al Rolled Products, Bonn, Germany for direct financial support.

REFERENCES

Abid, T., Boubertakh, A., & Hamamda, S. (2010). Effect of pre-aging and maturing on the precipitation hardening of an Al–Mg–Si alloy. *Journal of Alloys and Compounds, 490*, 166-169. https://doi.org/10.1016/j.jallcom.2009.10.096

Andersen, S. J., Zandbergen, H. W., Jansen, J., Træholt, C., Tundal, U., & Reiso, O. (1998). The crystal structure of the β" phase in Al-Mg-Si alloys. *Acta Materialia, 46*, 3283-3298. https://doi.org/10.1016/S1359-6454(97)00493-X

Andersen, S. J., Marioara, C. D., Vissers, R., Frøseth, A. L., & Derlet, P. (2004). Precipitate structures in Al-Mg-Si Alloys related by Si-network. *Proceedings of the 13th European Microscopy Congress, 2*, 599-600.

Andersen, S. J., Marioara, C. D., Frøseth, A., Vissers, R., & Zandbergen, H. W. (2005). Crystal structure of the orthorhombic U2-$Al_4Mg_4Si_4$ precipitate in the Al-Mg-Si alloy system and its relation to the β'

and β'' phases. *Materials Science and Engineering A, 390*, 127-138. https://doi.org/10.1016/j.msea.2004.09.019

Andersen, S. J., Marioara, C. D., Vissers, R., Frøseth, A., & Zandbergen, H. W. (2007). The structural relation between precipitates in Al-Mg-Si alloys and diamond silicon, with emphasis on the trigonal phase U1-$MgAl_2Si_2$. *Materials Science and Engineering A, 444*, 157-169. https://doi.org/10.1016/j.msea.2006.08.084

Andersen, S. J., Marioara, C. D., Friis, J., Bjørge, R., Du, Q., & Ringdalen, I. G. (2017). Directionality and column arrangement principles of precipitates in Al-Mg-Si-(Cu) and Al-Mg-Cu linked to line defect in Al. *Materials Science Forum, 877*, 461-470. https://doi.org/10.4028/www.scientific.net/MSF.877.461

Aruga, Y., Kozuka, M., Takaki, Y., & Sato, T. (2014). Evaluation of solute clusters associated with bake-hardening response in isothermal aged Al-Mg-Si alloys using a three-dimensional atom probe. *Metallurgical and Materials Transactions A, 45*, 5906-5913. https://doi.org/10.1007/s11661-014-2548-y

Aruga, Y., Kozuka, M., Takaki, Y., & Sato, T. (2015). Formation and reversion of clusters during natural aging and subsequent artificial aging in an Al-Mg-Si alloy. *Materials Science and Engineering A, 631*, 86-96. https://doi.org/10.1016/j.msea.2015.02.035

Aruga, Y., Kozuka, M., & Sato, T. (2018). Formulation of initial artificial age-hardening response in an Al-Mg-Si alloy based on the cluster classification using a high-detection-efficiency atom probe. *Journal of Alloys and Compounds, 739C*, 1115-1123. https://doi.org/10.1016/j.jallcom.2017.10.220

Engler, O., Schäfer, C., & Myhr, O.R. (2015). Effect of natural ageing and pre-straining on strength and anisotropy in aluminium alloy AA 6016. *Materials Science and Engineering A,* 639, 65-74. https://doi.org/10.1016/j.msea.2015.04.097

Engler, O., Schäfer, C., Brinkman, H.-J., Marioara, C.D., Kozuka, M., Shishido, H., & Aruga, Y. (2017). A combined TEM and atom probe approach to analyse the early stages of age hardening in AA 6016. *Materials Science Forum, 877*, 231-236. https://doi.org/10.4028/www.scientific.net/MSF.877.231

Frank, F. C. & Kasper, J. S. (1958). Complex alloy structures regarded as sphere packings. *Acta Crystallographica, 11*, 184-190. https://doi.org/10.1107/S0365110X58000487

Hasting, H. S., Frøseth, A. G., Andersen, S. J., Vissers, R., Walmsley, J. C., Marioara, C. D.,…Holmestad, R. (2009). Composition of β" precipitates in Al-Mg-Si alloys by atom probe tomography and first principles calculations. *Journal of Applied Physics, 106*, 123527. https://doi.org/10.1063/1.3269714

Kovarik, L., Gouma, P. I., Kisielowski, C., Court, S. A., and Mills, M. J. (2004). A HRTEM study of metastable phase formation in Al-Mg-Cu alloys during artificial aging. *Acta Materialia, 52*, 2509-2520. https://doi.org/10.1016/j.actamat.2004.04.041

Kresse, G., & Hafner, J. (1993). Ab initio molecular dynamics for liquid metals. *Physical Review B, 47*, 558-561. https://doi.org/10.1103/PhysRevB.47.558

Kresse, G., & Furthmuller, J. (1996). Efficiency of ab initio total energy calculations for metals and semiconductors using a plane wave basis set. *Computational Materials Science, 6*, 15–50. https://doi.org/10.1016/0927-0256(96)00008-0

Marioara, C. D., Andersen, S. J., Zandbergen, H. W., & Holmestad R. (2005). The influence of alloy composition on precipitates of the Al-Mg-Si system. *Metallurgical and Materials Transactions A, 36*, 691-702. https://doi.org/10.1007/s11661-005-1001-7

Marioara, C. D., Andersen, S. J., Røyset, J., Reisø, O., Gulbrandsen-Dahl, S., Nicolaisen, T. E.,…Holmestad, R. (2014). Improving thermal stability in Cu-containing Al-Mg-Si alloys by

precipitate optimization. *Metallurgical and Materials Transactions A, 45*, 2938-2949. https://doi.org/10.1007/s11661-014-2250-0

Matsuda, K, Kawai, A., Watanabe, K., Lee, S., Marioara, C. D., Wenner, S.,…Ikeno, S. (2017). Extra electron diffraction spots caused by fine precipitates formed at the early stage of aging in Al-Mg-X (X=Si, Ge, Zn)-Cu alloys. *Materials Transactions, 58*, 167-175. https://doi.org/10.2320/matertrans.L-M2016839

Murali, S., Arunkumar, Y., Chetty, P. V. J., Raman, K. S., & Murthy K. S. S. (1997). The effect of preaging on the delayed aging of Al-7Si-0.3Mg. *JOM-Journal of the Minerals Metals & Materials Society, 49*, 29-33. https://doi.org/10.1007/BF02915475

Nellist, P. D., & Pennycook, S. J. (2000). The principles and interpretation of annular dark-field Z-contrast imaging. *Advances in Imaging and Electron Physics, 113*, 147-203. https://doi.org/10.1016/S1076-5670(00)80013-0

Pashley, D. W., Rhodes, J. W., & Sendorek, A. (1966). Delayed ageing in Aluminium-Magnesium-Silicon alloys - effect on structure and mechanical properties. *Journal of the Institute of Metals, 94*(2), 41-49.

Perdew, J. P., Burke, K., & Ernzerhof, M. (1996). Generalized gradient approximation made simple. *Physical Review Letters, 77*(18), 3865-3868. https://doi.org/10.1103/PhysRevLett.77.3865

Rose, H. (2010). Theoretical aspects of image formation in the aberration-corrected electron microscope. *Ultramicroscopy, 110*(5), 488-499. https://doi.org/10.1016/j.ultramic.2009.10.003

Røyset, T., Stene, T., Sæter, J. A., & Reiso, O. (2006). The effect of intermediate storage temperature and time on the age hardening response of Al-Mg-Si alloys. *Materials Science Forum, 519-521*, 239-244. https://doi.org/10.4028/www.scientific.net/MSF.519-521.239

Sato, T., Kojima, Y., & Takahashi, T., (1982). Modulated Structures and GP Zones in Al-Mg Alloys. *Metallurgical and Materials Transactions A, 13*, 1373-1378. Retrieved from https://link.springer.com/content/pdf/10.1007/BF02642874.pdf

Serizawa, A., Hirosawa, S., & Sato, T. (2008). Three-dimensional atom probe characterization of nanoclusters responsible for multistep aging behavior of an Al-Mg-Si alloy. *Metallurgical and Material Transactions A, 39*(2), 243-251. https://doi.org/10.1007/s11661-007-9438-5

Vissers, R., van Huis, M. A., Jansen, J., Zandbergen, H. W., Marioara, C. D., & Andersen, S. J. (2007). The crystal structure of the β' phase in Al-Mg-Si alloys. *Acta Materialia, 55*, 3815-3823. https://doi.org/10.1016/j.actamat.2007.02.032

Vissers, R., Marioara, C. D., Andersen, S. J., & Holmestad, R. (2008). Crystal structure determination of the B' phase in Al-Mg-Si alloys by combining quantitative electron diffraction and ab-initio calculations. *Aluminium Alloys (Proceedings of ICAA11), 2*, 1263-1269.

Wenner, S., Marioara, C. D., Andersen, S. J., & Holmestad, R. (2012). Effect of room temperature storage time on precipitation in Al-Mg-Si(-Cu) alloys with different Mg/Si ratios. *International Journal of Materials Research, 103*(8), 948-954. https://doi.org/10.3139/146.110795

Yamada, K., Sato, T., & Kamio, A. (2000). Effects of quenching conditions on two-step aging behavior of Al-Mg-Si alloys. *Materials Science Forum, 331-337*, 669-674. https://doi.org/10.4028/www.scientific.net/MSF.331-337.669

Yamazaki, T., Kawasaki, M., Watanabe, K., Hashimoto, I., & Shiojiri M. (2002). Effect of small crystal tilt on atomic-resolution high-angle annular dark field STEM imaging. *Ultramicroscopy 92*, 181-189. https://doi.org/10.1016/S0304-3991(02)00131-6